ARCHIVIO ISTITUZIONALE DELLA RICERCA

Alma Mater Studiorum Università di Bologna
Archivio istituzionale della ricerca

Online EIS and Diagnostics on Lithium-Ion Batteries by means of Low-power Integrated Sensing and Parametric Modeling

This is the final peer-reviewed author's accepted manuscript (postprint) of the following publication:

Published Version:
Crescentini, M., De Angelis, A., Ramilli, R., De Angelis, G., Tartagni, M., Moschitta, A., et al. (2021). Online EIS and Diagnostics on Lithium-Ion Batteries by means of Low-power Integrated Sensing and Parametric Modeling. IEEE TRANSACTIONS ON INSTRUMENTATION AND MEASUREMENT, 70, 1-11 [10.1109/TIM.2020.3031185].

Availability:
This version is available at: https://hdl.handle.net/11585/777605 since: 2021-01-05

Published:

DOI: http://doi.org/10.1109/TIM.2020.3031185

Terms of use:

Some rights reserved. The terms and conditions for the reuse of this version of the manuscript are specified in the publishing policy. For all terms of use and more information see the publisher's website.

This item was downloaded from IRIS Università di Bologna (https://cris.unibo.it/).
When citing, please refer to the published version.

(Article begins on next page)

16 September 2026

This is the final peer-reviewed accepted manuscript of:

M. Crescentini *et al.*, "Online EIS and Diagnostics on Lithium-Ion Batteries by means of Low-power Integrated Sensing and Parametric Modeling," *IEEE Trans. Instrumentation & Measurement*, in-press, 2020

The final published version is available online at DOI:

https://doi.org/10.1109/TIM.2020.3031185

Rights / License:

The terms and conditions for the reuse of this version of the manuscript are specified in the publishing policy. For all terms of use and more information see the publisher's website.

This item was downloaded from IRIS Università di Bologna (https://cris.unibo.it/)

When citing, please refer to the published version.

Online EIS and Diagnostics on Lithium-Ion Batteries by means of Low-power Integrated Sensing and Parametric Modeling

M. Crescentini, *Member, IEEE,* A. De Angelis, *Member, IEEE,* R. Ramilli, G. De Angelis, M. Tartagni, *Member, IEEE,* A. Moschitta, *Member, IEEE,* P. A. Traverso, *Member, IEEE,* P. Carbone, *Fellow Member, IEEE*

***Abstract*—This paper presents a compact measurement system for electrochemical impedance spectroscopy (EIS) on lithium-ion battery (LIB). The system is composed of a vector impedance analyzer (VIA) and state parameter estimation. The VIA architecture is based on delta-sigma digital-to-analog and analog-to-digital conversions to achieve the compactness, low-power consumption, and high resolution required to be potentially integrated within a battery cell. The estimation of state parameters is based on equivalent circuit models and the solution of non-linear optimization problems. The proposed measurement system aims at the integration of complex measurement features directly into the battery cell to allow online and real-time diagnostic of the battery cell. A prototype of the compact measurement system was realized to assess the proposed approach. Experimental results are provided and validated by comparison with a reference laboratory instrument, showing good agreement. The VIA prototype is experimentally tested in both the online monitoring and aging monitoring of a commercial LIR2032 LIB cell. The modeling approach is applied to the experimental data provided by the VIA prototype, showing a good fit of the data. Moreover, parameters of the equivalent circuit models are extracted from the experimental data provided by the VIA prototype and identify trends related to the state of charge of the battery.**

***Index Terms*— Battery; Battery management; Electrochemical impedance spectroscopy (EIS); Electronic instrument; Impedance measurement; in-situ; Lithium-ion batteries; Online diagnostic; Modeling**

I. INTRODUCTION

Batteries have attracted considerable research interest in recent years due to their increasing usage in a variety of applications. Such applications, which were once limited to low-power systems such as portable electronics, are recently expanding towards higher energy scenarios, including electrical vehicles and energy storage systems [1]. In this context, lithium-ion batteries (LIBs) are among the most commonly employed, thanks to their high energy density and compact size [2].

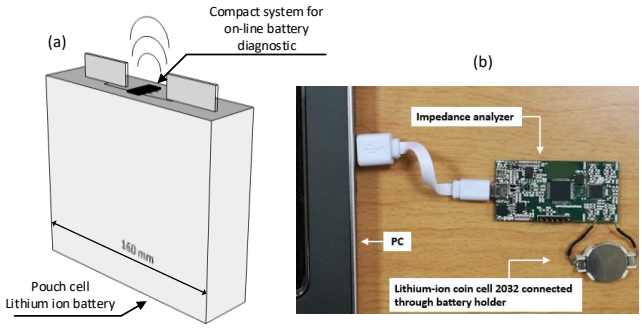

Fig. 1 (a) Smart battery concept in which a compact system for online battery diagnostics is integrated directly on the LIB cell. (b) Photograph of the prototype discussed in this paper.

In order to ensure the safe operation of lithium-ion batteries and improve efficiency, battery management systems typically employ parametric battery models. By identifying the model parameters, it is possible to indirectly evaluate the State of Charge (SoC) and the State of Health (SoH) of the battery. Furthermore, the models allow for simulating the battery behavior under different SoC and SoH conditions, allowing to develop and test algorithms for battery management [3]. The model parameters are typically identified by processing measurement data obtained by electrochemical impedance spectroscopy (EIS) [4]. To obtain EIS data efficiently, broadband and narrowband measurement systems have been

This work was supported in part by the Italian Ministry for Education, University and Research (MIUR) under the program "Dipartimenti di Eccellenza" (2018-2022)

A. De Angelis, A. Moschitta and P. Carbone are with the Department of Engineering, University of Perugia, Italy. {alessio.deangelis, antonio.moschitta, paolo.carbone}@unipg.it.

G. De Angelis is with Regione Umbira, Perugia, Italy. ing.guidodeangelis@gmail.com

M. Crescentini, M. Tartagni and P.A. Traverso are with the Department of Electrical, Electronic and Information Engineering (DEI) "G. Marconi" University of Bologna, Italy. {m.crescentini, marco.tartagni, pierandrea.traverso}@unibo.it

R. Ramilli is with the Advanced Research Center on Electronic Systems (ARCES), University of Bologna, Italy. roberta.ramilli2@unibo.it

This item was downloaded from IRIS Università di Bologna (https://cris.unibo.it/)

When citing, please refer to the published version.

proposed in the literature [5]. In the former system, broadband signals are fed to the battery input and excite a wide range of frequencies simultaneously. Such signals may be implemented efficiently by using binary or ternary sequences that are designed specifically for system identification [6] [7]. The latter system consists in exciting the battery by using a narrowband signal and spanning the center frequency of this excitation. The narrowband measurement system is intrinsically slower but with superior resolution [8], [9], [10]. Most EIS instruments are benchtop devices and cannot be applied directly on the field to characterize batteries while they are operating. This limits the application of the parametric models to off-line characterization performed only in specialized laboratories. However, the capability of measuring the impedance of a battery in a cost-effective, efficient, and fast manner is crucial for the safe and efficient operation of lithium-ion batteries, thus motivating research in this area.

In the literature, the terms "*in-situ*" and "*in-operando*" monitoring usually refer to the monitoring of the battery cell while it undergoes a charge/discharge process but under controlled conditions, that are achievable only in laboratories [11]. This is a powerful technique that allows fast implementation and characterization of novel battery cell chemistries [12]. Alternatively, the term "*in-situ*" EIS monitoring refers to the EIS characterization during charge/discharge of the battery but having the cell disconnected from the load during the EIS test [13]. These concepts are considerably different from the online monitoring concept targeted by this paper, in which the EIS should be performed while the battery is working and it is connected to a load. There are few works in the literature that recognize the importance of online battery monitoring and are pushing towards this goal. Itagaki et al. [14] demonstrated the feasibility of online EIS monitoring but they used lab-grade galvanostatic instrument in laboratory environment. Koleti et al. [15] proposed the online EIS monitoring as a way to detect lithium plating while the battery is working but, again, they rely on standard laboratory instruments. Given the importance and potential impact of online EIS monitoring, a number of research groups are developing EIS measurement systems that can be easily integrated in battery-powered applications. The majority of the proposed architectures exploit the power converter embedded into the application to generate the sinusoidal excitation while the readout/receiving channel is rather standard [16]–[20]. This approach is not general since it strongly depends on the final application, moreover, it is prone to the distortion and noise generated by the DC-DC converter used as the excitation generator. Howey et al., as well as Troltzsch and Kanoun [21], [22], proposed a multi-sine approach based on direct-digital synthesizers to stimulate the battery but the measurement system relies on off-the-shelf component, thus they do not meet the miniaturization and low-power requirements. Gong et al. [23] proposed a battery management system (BMS) integrated with an EIS measurement system into a single cell supervisor (SCS) IC. However, the EIS system excites the battery with a high-amplitude current sinewave to achieve good SNR, consuming a large amount of power.

This paper proposes a compact system able to gather EIS data and estimate the target parameters of interest by using suitable electrical models. The proposed system could potentially operate "*online*", that is while the battery is under operation, thanks to its compactness, low power consumption, and isolation from the battery under test. Compactness and *online* operation of the proposed system could enable the development of built-in battery management systems, fault warning solutions, and real-time diagnostics. The final aim of this work is to enable the integration of complex and real-time measurement features directly into the battery cell to allow the development of the smart battery concept of Fig. 1.

As a first step towards this goal, a prototype of the system is implemented and compared with a commercial benchtop instrument used as the gold standard for EIS. The prototype consists of a vector impedance analyzer (VIA) realized as a small printed circuit board. The VIA core is implemented as an application-specific integrated circuit (ASIC) to reduce the size and allow energy-efficient operations. This device measures the battery impedance at several frequencies with a very small form factor and low power consumption. Potentially, all the components in the realized prototype could be integrated into a single ASIC and embedded inside the battery cell itself, thus allowing for efficient monitoring of battery parameters.

The remainder of this paper is organized as follows. Section II focuses on the vector impedance analyzer, presenting the architecture, the calibration procedure, and experimental results. Subsequently, the usage of such experimental results for modeling and parameter identification purposes is investigated in Section III. Finally, conclusions are drawn in Section IV. This manuscript extends [24], presented at the 2020 I2MTC

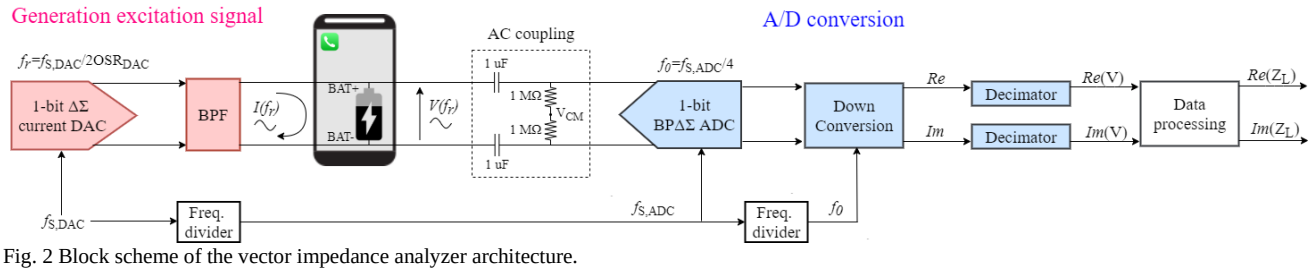

Fig. 2 Block scheme of the vector impedance analyzer architecture.

This item was downloaded from IRIS Università di Bologna (https://cris.unibo.it/)

When citing, please refer to the published version.

conference, by i) adding details and results of the calibration procedure, ii) validating the VIA in two case studies, iii) extracting model parameters from experimental EIS data and relating them to SoC levels.

II. The Vector Impedance Analyzer

A. Architecture

The VIA architecture is based on a delta-sigma (ΔΣ) digital-to-analog (D/A) converter for the generation of a narrowband AC excitation signal and a band-pass delta-sigma (BPΔΣ) analog-to-digital (A/D) converter for the acquisition and conversion of the response signal (Fig. 1) [8] [9]. The use of 1-bit ΔΣ D/A and A/D conversion architectures ensures very low-power consumption while preserving high resolution, thanks to the well-known oversampling and noise shaping. In addition, relatively power-hungry computational steps inherent to ΔΣ D/A conversion (e.g., noise shaping) are implemented off-line via software, with a considerable reduction in power consumption. These operations are realized just once, and the resulting bit sequence is simply pre-stored into the system memory. Following this approach, the 1-bit ΔΣ D/A is realized in hardware by just a 1-bit I/O port connected to a memory device. The 1-bit BPΔΣ A/D conversion is more power-efficient than conventional low-pass A/D conversion. It allows to replace non-linear and noisy analog mixers with a low-power digital down-conversion stage, which provides (after suitable filtering and decimation) full vector information on the battery impedance. Finally, the band-pass architecture of the A/D converter minimizes the in-band thermal noise, improving SNR.

The combination of ΔΣ D/A conversion with the implementation of BPΔΣ A/D conversion also allows real-time tuning of the operative excitation frequency f_r, so as to span the target portion of the frequency domain. More precisely, the frequency f_r of the excitation sine wave can be tuned in real-time by simply varying the D/A converter sampling frequency $f_{S,DAC}$, since these two frequencies are related by the following equation:

$$f_r = \frac{f_{S,DAC}}{2 \cdot OSR_{DAC}}, \quad (1)$$

where OSR_{DAC} is the chosen oversampling ratio of the ΔΣ D/A converter implemented in the architecture.

BPΔΣ A/D conversion works in a similar way with respect to the conventional low-pass ΔΣ technique, but benefits from the bandpass nature of the signal to be acquired to obtain higher OSR values (thus, more effective noise shaping) with lower sampling frequencies (i.e., lower consumption). In this case, the oversampling ratio of the BPΔΣ A/D converter is defined as the ratio between the Nyquist frequency $f_{S,ADC}/2$ and the bandwidth B_W of the acquired signal:

$$OSR_{ADC} = \frac{f_{S,ADC}}{2 \cdot B_W}, \quad (2)$$

in which $B_W << f_0$, which is the center frequency of the BPΔΣ. The latter can be parametrized to the sampling frequency $f_{S,ADC}$ through the linear relation:

$$f_{S,ADC} = P \cdot f_0, \quad (3)$$

where P is a factor depending on the actual implementation. A clever choice is P = 4 because it simplifies the electronic implementation of the BPΔΣ. Since $f_{S,ADC}$ is internally generated from $f_{S,DAC}$ as follows:

$$f_{S,ADC} = \frac{f_{S,DAC}}{K_{DIV}}, \quad (4)$$

then the frequency equalization is assured by the combination of (1) and (3). The factor K_{DIV} is set by the hardware frequency divider and is a power of two for simple implementation. Therefore, the target frequency spectrum can be easily spanned only by sweeping $f_{S,DAC}$, while the frequency equalization of the D/A and A/D conversions is assured by construction.

The DC voltage of the battery under test is decoupled both from the D/A and A/D converters. The 1 Hz - 10 kHz band-pass filter (BPF), placed in between the D/A converter and the battery, removes the high-frequency noise of the ΔΣ excitation and avoids slow-varying DC-like currents from battery to D/A converter without affecting the normal behavior of the battery and of the device powered by the battery itself. The bandwidth of the BPF is chosen with the twofold aim of *i)* not limiting the frequency sweep required to estimate the interesting portion of the electrochemical impedance (EI) spectrum of the battery under test, and *ii)* minimizing the noise associated with the ΔΣ excitation. The AC coupling on the A/D side separates the power supply domain of the VIA from the battery, to prevent spurious currents through the electrostatic discharge (ESD) circuits placed on the input of the BPΔΣ. The AC coupling circuit consists of two 1-μF capacitors in series to the battery to block the DC voltage, and of two 1-MΩ resistors to set the common-mode DC input voltage of the A/D converter.

The proposed VIA can be used to monitor the EI of the battery *online*, i.e., even while the latter is supplying a circuital load. The current excitation $I(f_r)$ provided by the VIA is AC-injected into the battery through the BPF and adds to the slow-varying current supplied by the battery itself. The AC excitation will flow through the battery and not through the load because of the very low input impedance of the battery itself. The AC voltage across the battery due to slow variations of the load is rejected by the intrinsic frequency-locked operation of the VIA. The proposed VIA architecture is appropriate to be

This item was downloaded from IRIS Università di Bologna (https://cris.unibo.it/)

When citing, please refer to the published version.

implemented in very compact dimensions, down to a few mm^2, by exploiting microelectronic techniques. This capability, together with the low-power consumption and the electrical isolation from the battery, allows to integrate the VIA with every battery module, or even at the very battery cell level, opening new perspectives in battery smart sensing/functionality applications.

B. Implemented prototype

To assess the functionalities of the VIA architecture and its applicability to EIS on battery modules, a prototype of the VIA is realized on a 3-cm x 6-cm PCB board (Fig. 1-b). The main sub-circuits are realized in a CMOS ASIC, while ancillary digital sub-circuits are implemented onto a microcontroller (μC). This approach does not achieve fully optimized compactness of the prototype but guarantees the best resolution and accuracy together with a good level of flexibility and testability. On one hand, the CMOS implementation of the analog front-end ensures better noise immunity and lower parasitics, improving prototype robustness and accuracy. On the other hand, the implementation of the digital algorithms in the microcontroller allows for the optimization of the measurement parameters to the target application. Following this approach, the prototype can be programmed by choosing the amplification gain as well as the amplitude and the frequency of the excitation current signals.

The implemented VIA prototype can operate up to the 45-kHz frequency range. In the following tests, however, the excitation signal will discretely span only the 12 Hz – 3 kHz range by twenty-five arbitrarily chosen frequency points f_r. For each excitation frequency, the impedance estimate corresponds to the average over 30 samples in order to lower the random noise that affects the single-sample reading due to technological issues. Thus, a low-frequency limit of 12 Hz has been selected to both preserve a suitably short measurement time, that assures the responsiveness of the diagnostics and the time-invariance of the battery during the frequency sweep, and maximize the SNR of each impedance estimate. The high-frequency limit has been chosen, instead, according to the impedance behavior of the DUTs, which becomes purely inductive (i.e., not significant for diagnostics) at tens of kHz. In the following sub-sections, the VIA prototype is operated by setting the sine wave amplitude to the maximum value of 1 mA and the amplification gain of the front-end to the value of 2, in order to enable the VIA to detect low impedance changes, typical of LIB cells.

The prototype consumes a maximum of 500 mW when it generates the maximum excitation frequency of 45 kHz, but the power consumption lowers to 100 mW when operating at f_r = 1 kHz. It is worth noticing that most of the power is dissipated by the general-purpose μC while the ASIC consumes only 1.45 mW. Future implementations of the VIA may integrate all the blocks shown in Fig. 2 into a single ASIC to further boost the performance, minimize the power consumption as well as the form factor.

C. Calibration procedure

The prototype needs a calibration procedure to cope with non-idealities of the VIA architecture. Specifically, the receiver, i.e., the A/D conversion chain, is characterized by an input-referred offset on the measured voltage that corrupts the impedance estimate with an offset term $Z_{OS}(f_r)$. This term depends on the excitation frequency because of the chosen implementation of the BPΔΣ converter [8]. Also, the wires connecting the VIA to the battery add their own impedance as an offset term. Moreover, the analog passive filters used in the acquisition chain (i.e., both the BPF and the AC coupling circuits) have not a flat frequency response and are affected by the impedance of the battery, thus the entire VIA suffers from frequency dispersion of its gain parameter and non-linearity errors, which are accounted for by a non-linear transfer term $H(f_r,Z)$, where Z is the impedance of the battery. The above non-idealities are dealt with by modeling the output of the VIA Z_L as:

$$Z_L(f_r) = Z_{OS}(f_r) + H(f_r, Z) \cdot Z(f_r) \quad (5)$$

where all the terms in the equation are complex functions of the excitation frequency f_r, thus, both amplitude and phase perturbations are considered.

The calibration of the VIA follows a simplified VNA-like procedure, where only short and load configurations are implemented since only two non-ideality parameters are present in the measurement model of (5). Offset parameter $Z_{OS}(f_r)$ is estimated by shorting the input of the receiver and spanning all the implemented frequency points. The load configuration of the calibration procedure is performed by using the target battery cell as a standard input load, since the measurement system is conceived to be integrated within a specific battery cell to be monitored over its lifetime. The reference value of the impedance spectrum of the battery is measured by using the

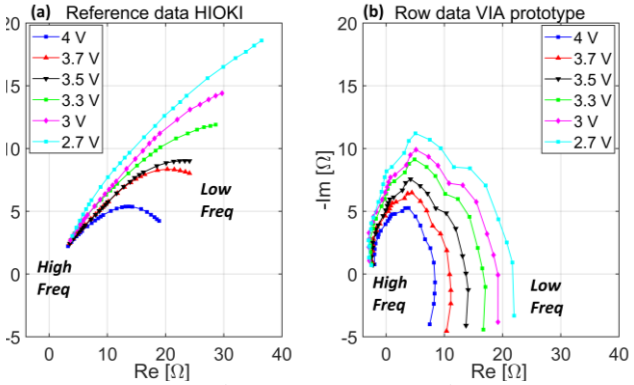

Fig. 3 Cole-Cole plots of the impedance spectra of the target battery cell LIR2032 at various V_{OC} values recorded during the calibration procedure by (a) the HIOKI IM3590 reference instrument and (b) the proposed uncalibrated VIA prototype.

This item was downloaded from IRIS Università di Bologna (https://cris.unibo.it/)

When citing, please refer to the published version.

Hioki IM3590 Chemical Impedance Analyzer, which is a gold-standard instrument for battery EIS, with a rated accuracy of 3% of the reading for the impedance magnitude and 0.6° for the impedance phase. We considered a commercially available lithium-ion rechargeable coin cell (LIR2032) of chemistry lithium cobalt oxide ($LiCoO_2$) as target battery cell, in agreement with [2]. The battery has a weight of 2.5 g, nominal voltage of 3.6 V, and nominal capacity of 45 mAh. The non-linear transfer function $H(f_r,Z)$ is actually only mildly dependent on the impedance spectrum of the battery under test $Z(f)$, since the system is calibrated directly on the battery target, for which impedance variations are relatively small and trigger only partially the non-linearities of the VIA. Thus, for the following tests, it is reasonable to approximate $H(f_r,Z)$ with the linear calibration function $\hat{H}(f_r)$ computed as a least-square average over the complex impedance space of interest. For different DUTs, with larger impedance variations in the bandwidth of interest, the full $H(f_r,Z)$ can be extracted, and stored either by complex interpolation throughout the Z-region, or as a look-up table function.

The load calibration procedure is as in the following: first, the battery is charged until the voltage reaches the maximum value (4.1 V for the DUT in the example), then the battery is discharged using a resistive load until it reaches a specific target voltage. After 2 hours of relaxation time, the voltage of the battery becomes stable and this value is defined as the open-circuit voltage V_{OC}. The impedance spectrum of the battery is now measured by using the uncalibrated VIA prototype while the Hioki IM3590 is used as the reference instrument. The discharge process starts again in order to collect the impedance spectrum for different V_{OC} on a suitable grid (4 V, 3.7 V, 3.5 V, 3.2 V, 3V, and 2.7 V in the example). All the recorded impedance spectra are reported in Fig. 3, showing that, though the VIA prototype is able to detect the changes in the impedance spectrum due to the discharge process, the estimated spectra are distorted with respect to the reference ones. The calibration function $\hat{H}(f_r)$ is then estimated by solving the weighted least-squares (WLS) regression over the entire calibration space for each frequency point f_r, separately. The Cole-Cole plot, as well as the corresponding magnitude and argument plots, of $\hat{H}(f_r)$ are reported in Fig. 4, showing that the main perturbation introduced by the VIA prototype is a non-constant phase rotation.

All the impedance spectrum estimates $\hat{Z}(f_r)$ reported in the following sections have undergone the following calibration model:

$$\hat{Z}(f_r) = \frac{Z_L(f_r) - \hat{Z}_{OS}(f_r)}{\hat{H}(f_r)} \quad (6)$$

where $\hat{Z}_{OS}(f_r)$ and $\hat{H}(f_r)$ are extracted as explained above. The application of the calibration process to the uncalibrated datasets of Fig. 3 is reported in Fig. 5 and compared with the reference.

To evaluate the performance of the calibration procedure, the leave-one-out cross-validation procedure was applied within

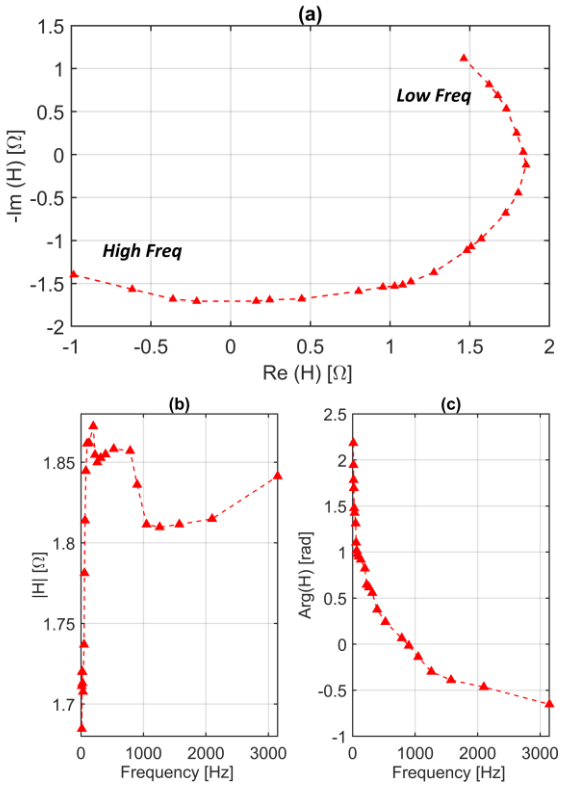

Fig.4 (a) Cole-Cole plot and (b-c) Bode diagrams of the VIA calibration function $\hat{H}(f_r)$ estimated with WLS regression. Both show a non-constant phase rotation introduced by the VIA prototype.

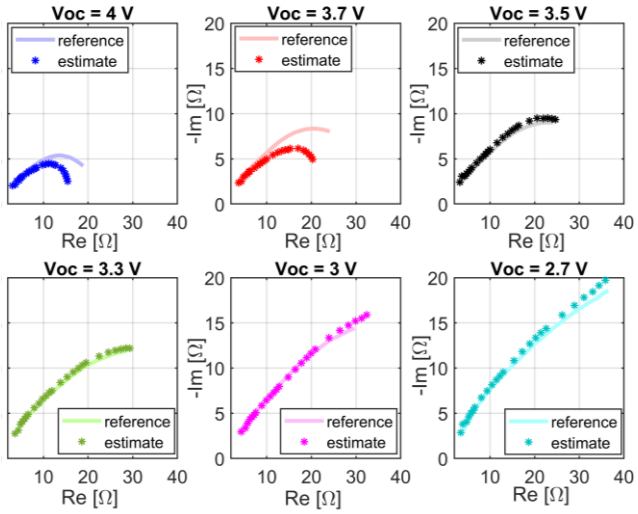

Fig. 5 Impedance spectra of the LIR2032 battery for the V_{OC} values collected during the calibration procedure. For each V_{OC} value the spectrum estimated by the calibrated VIA prototype is compared with the reference spectrum obtained by the Hioki IM3590.

This item was downloaded from IRIS Università di Bologna (https://cris.unibo.it/)

When citing, please refer to the published version.

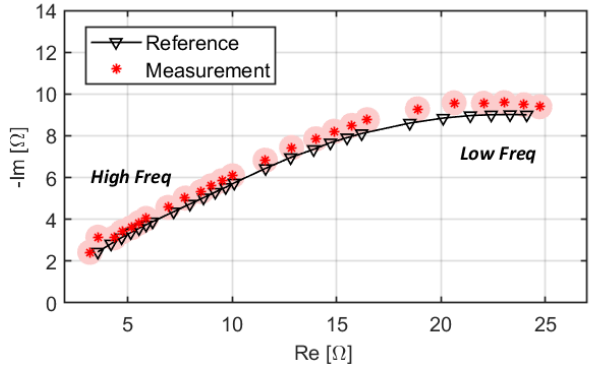

Fig.6 Comparison of the calibrated VIA with the reference instrument in the estimation of the impedance spectrum of the battery at V_{OC} = 3.5 V. The VIA is calibrated over the other 5 V_{OC} values reported in Fig. 5 while the curve at V_{OC} = 3.5 V is chosen as the out-calibration curve in the leave-one-out validation procedure. Shaded circles represent the mean complex RMS error of the VIA on the out-calibration curve.

the calibration data set. The results of the cross-validation are reported in Table I for all the combinations of the leave-one-out algorithm. Fig. 6 graphically expresses the quality of the calibration procedure by comparing the impedance spectrum of the battery at V_{OC} = 3.5 V (i.e. the out-of-calibration curve in the example) estimated by the calibrated VIA with the reference impedance spectrum. The shaded circles in the figure represent the mean complex RMS error introduced by the VIA on the out-calibration curve, according to Table I.

Tab. I Results of cross-validation of the calibration procedure

Out-calibration curve	rmse on calibration set (Ω)	rmse on the out curve (Ω)	rmse on the out curve (%rdg)
V_{OC} = 4 V	1.33	1.88	0.12
V_{OC} = 3.7 V	1.21	2.32	0.11
V_{OC} = 3.5 V	1.55	0.56	0.05
V_{OC} = 3.2 V	1.54	0.66	0.03
V_{OC} = 3 V	1.27	2.35	0.15
V_{OC} = 2.7 V	1.49	1.26	0.08
Mean value	1.40	1.50	0.09

D. *Online and aging monitoring*

The proposed VIA prototype is tested and validated in two different case-studies: *i)* online monitoring and *ii)* aging monitoring.

The first case-study aims to assess the capability of the VIA architecture to monitor the impedance spectrum of the battery online, that is while the battery is working. Fig. 7 shows the impedance spectra estimated by the calibrated VIA during the charge and discharge processes of the battery. The battery is connected to the Keithley 2450 source measurement unit (SMU) that emulates an electronic load with constant sink current of 1 mA, during the discharge cycle, and emulates a 1-mA constant current source, during the charge cycle. Fig. 7 clearly shows the evolution of the impedance spectrum during the charge/discharge cycle, validating the feasibility of online monitoring the state of the battery by means of EIS and demonstrating the online capability of the proposed VIA architecture. From Fig. 7 it is possible to infer that the online EI spectrum is different from the steady-state EI spectrum. That is completely reasonable since the online EI spectrum is an instant photograph of the battery state taking into consideration all the low-varying dynamic effects. It is also possible to infer from Fig. 7 that the EI spectrum responds in distinct ways to charge and discharge process, which agrees with other similar studies on different battery chemistries [25].

The second case study aims to validate the VIA architecture in a standard test for battery cells. In Fig. 8, the EI spectrum of the LIR2032 battery at V_{OC} = 4 V is measured at different stages of the battery life (i.e. at the 1st cycle, the 10th cycle, and the 20th cycle) by both the proposed VIA and the reference instrument.

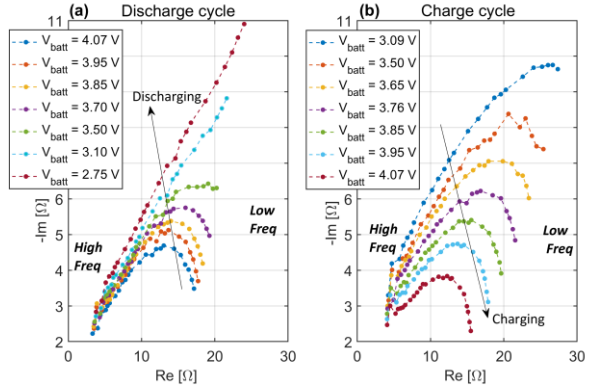

Fig.7 Online acquisition of the impedance spectrum of a LIR2032 battery by the calibrated VIA during the (a) discharge and (b) charge process by a constant DC current.

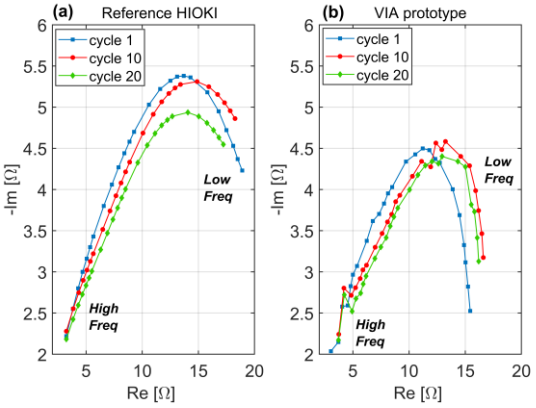

Fig.8 Monitoring of the aging of the LIB cell over 20 charge/discharge cycles at the maximum current of 40 mA. (a) EI spectra estimated by the reference instrument. (b) EI spectra estimated by the proposed VIA prototype.

This item was downloaded from IRIS Università di Bologna (https://cris.unibo.it/)

When citing, please refer to the published version.

The battery cell is cycled at the constant charge/discharge current of 40 mA. The standard aging protocol requires to perform a larger number of cycles but, due to time restriction, we can here report only the first 20 cycles. Thus, we performed the test at the maximum discharge current allowed by the LIB cell to speed up the aging processes. Fig. 8 shows the results of the test and compares the VIA prototype with the reference. The absolute values of the EI spectra estimated by the VIA are slightly different from the reference but still coherent with the rms error reported in Tab. I. Moreover, both the VIA prototype and the reference estimate the same aging trend of the EI spectra, confirming the validity of the proposed system.

III. Modeling

A. *Fitting to equivalent circuits*

The experimental results presented in Section II are used to identify the parameters of models based on equivalent circuits. These parametric models can then be employed by a battery management system to evaluate the SoC and SoH of a battery under test or for simulation purposes.

In the literature, the most commonly used equivalent circuit models are based on the Randles circuit or one of its variants (e.g., see[26]). Among these variants, to model the low-frequency behavior of the EIS curve, the Warburg element is often employed [27]. Instead, to model the high-frequency behavior, a resistor in series with an optional inductor is typically used. Regarding the mid-frequency behavior, one or more cells consisting of a parallel connection between a constant-phase element (CPE) and a resistor are used.

In this paper, two models are considered and compared. These models are denoted as Model 1, whose related circuit is shown in Fig. 9, and Model 2, which is depicted in Fig. 10. The impedance of Model 1 is given by [2]:

$$Z_1(s) = R_0 + \frac{R_1}{1+R_1Q_1s^{p_1}} + \frac{1}{Q_2s^{p_2}} \quad , \tag{7}$$

where Q_1 and p_1 are the parameters of CPE$_1$, Q_2 and p_2 those of CPE$_2$, $s = \mathrm{j}\omega$ is the Laplace variable, and ω is the angular frequency. The parameters of Model 1 can be grouped in vector θ_1 as follows:

$$\theta_1 = [R_0 \;\; R_1 \;\; Q_1 \;\; p_1 \;\; Q_2 \; p_2]^T \tag{8}$$

where T denotes the transpose operator. Furthermore, the impedance of Model 2 is:

$$Z_2(s) = sL + R_0 + \frac{R_1}{1 + R_1Q_1s^{p_1}} + \frac{R_2}{1 + R_2Q_2s^{p_2}} + \frac{A_w(1-j)}{s^{0.5}} \quad , \tag{9}$$

where A_w is the Warburg parameter. For Model 2, we define the parameter vector θ_2 as:

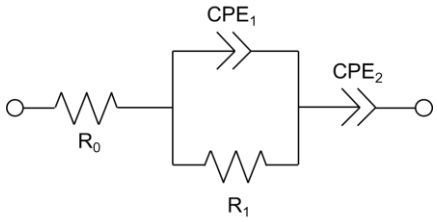

Fig. 9: Equivalent circuit of Model 1.

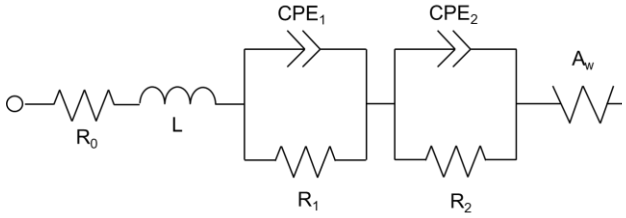

Fig. 10: Equivalent circuit of Model 2.

$$\theta_2 = [R_0 \;\; L \;\; R_1 \;\; Q_1 \;\; p_1 \;\; R_2 \; Q_2 \;\; p_2 \;\; A_w]^T \quad . \tag{10}$$

Let us assume that N measured values of the complex impedance $\tilde{Z}(s_i)$ are available at radian frequencies ω_i, with i=1,…,N. Based on these measurement results, the parameters of the models can be estimated by solving the following optimization problems [3]:

$$\min_{\theta_k} \sum_{i=1}^{N} (J_R^2 + J_I^2), \;\; k = 1,2 \tag{11}$$

where $J_R = Re\{\tilde{Z}(s_i)\} - Re\{Z_k(s_i, \theta_k)\}$, $J_I = Im\{\tilde{Z}(s_i)\} - Im\{Z_k(s_i, \theta_k)\}$, and θ_k indicates the vector of the parameters to be estimated, with k=1 in the case of Model 1, and k=2 for Model 2. These optimization problems are nonlinear in the parameters. Therefore, they can be solved using iterative numeric procedures that consider the constraints on some parameters and require an initial guess of their values.

This item was downloaded from IRIS Università di Bologna (https://cris.unibo.it/)

When citing, please refer to the published version.

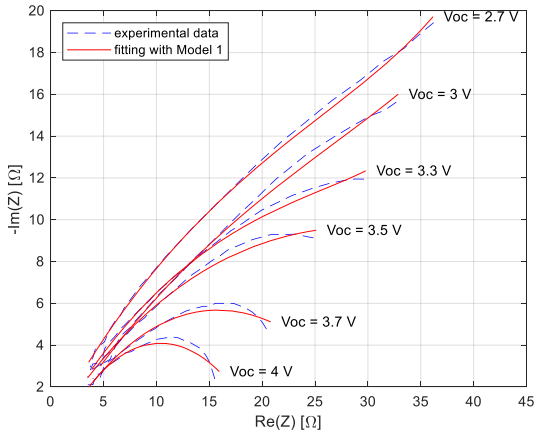

Fig. 11: Fitting results obtained using Model 1 on experimental data acquired by the calibrated VIA for different values of the open-circuit voltage Voc. The RMSE between the experimental data and the fitted curves is 0.22 Ω.

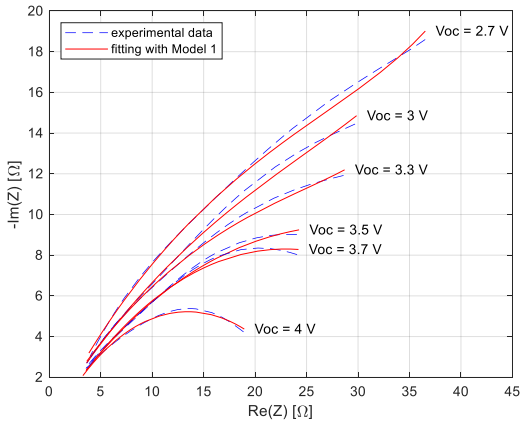

Fig. 12. Fitting results of Model 1 on experimental data acquired by the reference instrument Hioki IM3590 for different values of the open-circuit voltage Voc. The RMSE between the experimental data and the fitted curves is 0.17 Ω.

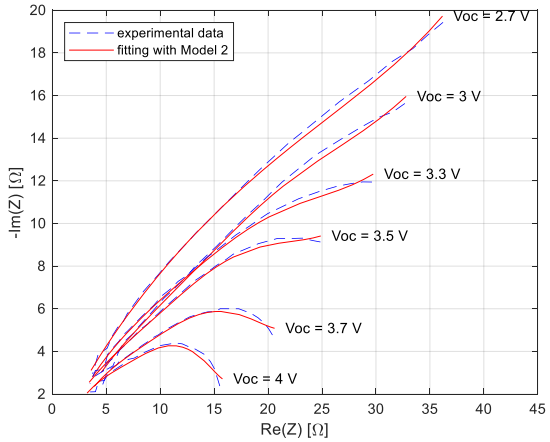

Fig. 13: Fitting results obtained using Model 2 on experimental data acquired by the calibrated VIA for different values of the open-circuit voltage Voc. The RMSE between the experimental data and the fitted curves is 0.17 Ω.

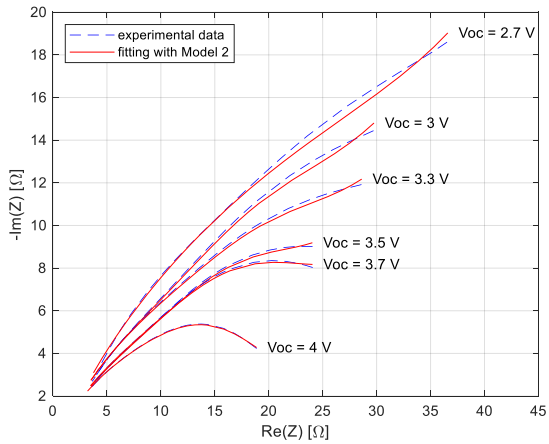

Fig. 14: Fitting results of Model 2 on experimental data acquired by the reference instrument Hioki IM3590 for different values of the open-circuit voltage Voc. The RMSE between the experimental data and the fitted curves is 0.12 Ω.

In this paper, the initialization for Model 1 is derived by observing the EIS data at different frequency ranges, based on the procedure described in [3]. Specifically, the initial value of R_0 is the high-frequency intercept with the horizontal axis, R_1 and Q_1 are initialized as the real and imaginary parts of the impedance at the maximum of the mid-frequency semicircle, respectively, and p_1 and p_2 are initialized at 0.5, which is a common value used in the literature [2]. An arbitrary initial value of Q_2=10 was used, since it was found empirically that the minimization procedure is not sensitive to the initial value of Q_2. The cost function for Model 1 is minimized using a trust region reflective algorithm [28]. For Model 2, a multi-start initialization is performed. In particular, 100 random initial conditions are generated, the cost function is minimized for each initial condition using a trust region reflective algorithm, and the parameter values that provide the lowest value of the cost function are selected.

Fitting Model 1 to data obtained by the realized VIA yields the curves shown in Fig. 11. A good agreement may be observed between experimental data and fit. Moreover, for evaluation and reference purposes, Model 1 is fitted also to data obtained by the reference instrument, Hioki IM3590, as shown in Fig. 12. By comparing the fitting results of Fig. 11 with those of Fig. 12, it is possible to notice that the behavior of the fitted curves is similar and that data from the reference instrument result in a better fit (RMSE of 0.17 Ω vs 0.22 Ω). Moreover, fitting Model 2 to data obtained by the realized VIA and the reference instrument yields the curves shown in Fig. 13 and 14, respectively. It can be noticed that Model 2 provides a better fit with respect to Model 1.

B. Effect of SoC on model parameters

Published results show that the parameters' values extracted from circuit models are related to performance indicators, such as SoC and SoH [29] [30] [22]. Specifically, in [29], a computational model based on multiple constant-phase

This item was downloaded from IRIS Università di Bologna (https://cris.unibo.it/)

When citing, please refer to the published version.

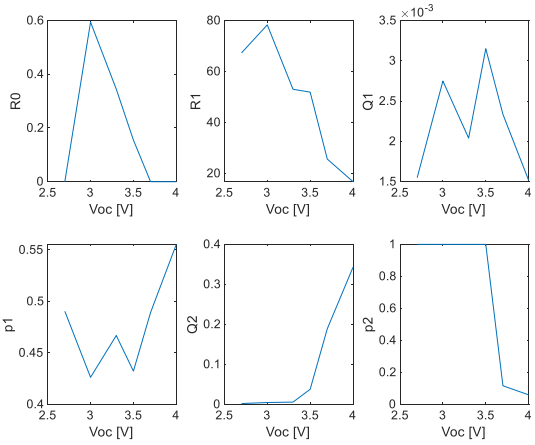

Fig. 15 – Behavior of the estimated parameters of Model 1 for varying values of the open-circuit voltage Voc (VIA).

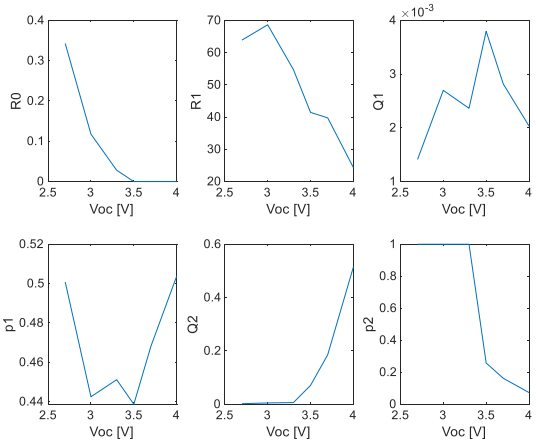

Fig. 16 – Behavior of the estimated parameters of Model 1 for varying values of the open-circuit voltage Voc (reference instrument Hioki IM3590

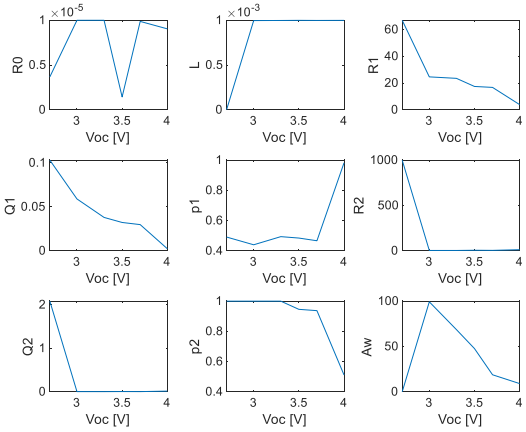

Fig. 17 – Behavior of the estimated parameters of Model 2 for varying values of the open-circuit voltage Voc (proposed VIA).

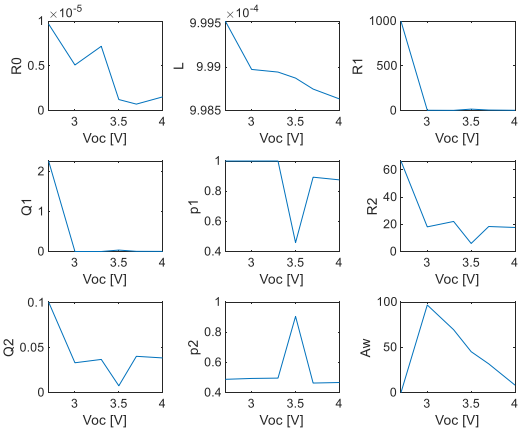

Fig. 18 – Behavior of the estimated parameters of Model 2 for varying values of the open-circuit voltage Voc (reference instrument Hioki IM3590).

elements (CPEs) is employed for fitting EIS data. It is shown that several model parameters, namely the series resistance and the exponent of a CPE, decrease when SoC increases. Furthermore, in [30], the SoH of lithium-polymer batteries is estimated with an error in the order of 4%. This estimate is based on the relation between SoH and the value of ohmic resistance, which is obtained by fitting the equivalent circuit model to EIS measurement results. Moreover, in [22], EIS is performed between 1 Hz and 2 kHz using broadband current excitation and then employed for SoC estimation. It is shown that the CPE admittance parameter exhibits a decreasing behavior with increasing SoC.

To study the relation between model parameters and SoC, we apply our modeling strategy to the experimental EIS data of Fig. 5. In particular, the behavior of the estimated parameters of Model 1 for several values of the open-circuit voltage is shown in Fig. 15 and Fig. 16, for the VIA and reference, respectively.

The estimated Model 1 parameters obtained when processing data from the reference instrument exhibit the same general behavior as those obtained when processing the VIA data. A decreasing trend of the parameter R_1 with increasing V_{OC} is observed, as well as an increasing trend of Q_2. This suggests that the VIA correctly identifies trends in the parameters, even though the lowest measurement frequency is relatively high (12 Hz) thus allowing for fast and online measurement of the parameters. Furthermore, trends in the parameters could be exploited to relate model parameters to SoC, similarly to the conclusions obtained in [28], [29].

Figs. 17 and 18 show the behavior of the estimated parameters of Model 2. It can be observed that the behavior of the estimated parameters for varying V_{OC} is not consistent, namely, the parameters obtained when processing data from the reference instrument show different behavior than those obtained using the proposed VIA. Furthermore, the behavior is generally not monotonic. This indicates that Model 2 is not adequate for describing the experimental data acquired for the used coin cell sample.

This item was downloaded from IRIS Università di Bologna (https://cris.unibo.it/)

When citing, please refer to the published version.

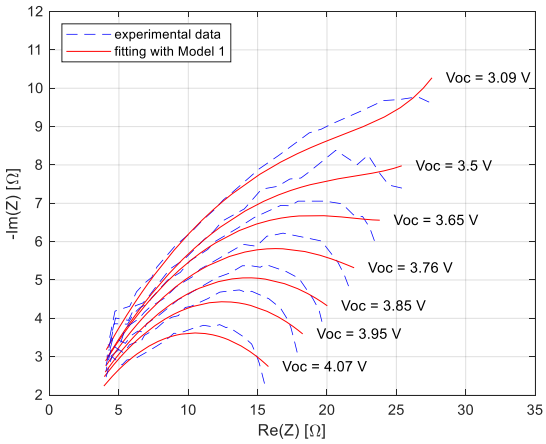

Fig. 19 – Fitting of online monitoring data on a charging battery, using Model 1.

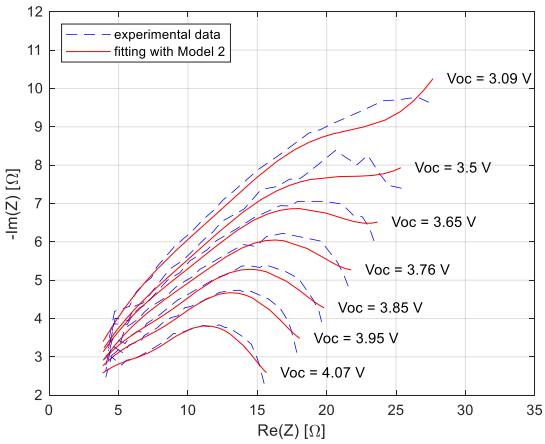

Fig. 20 – Fitting of online monitoring data on a charging battery, using Model 2.

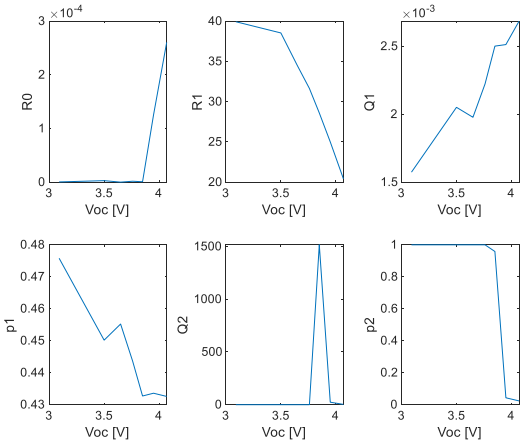

Fig. 21 – Behavior of the estimated parameters of Model 1 for the online monitoring data in the charging phase.

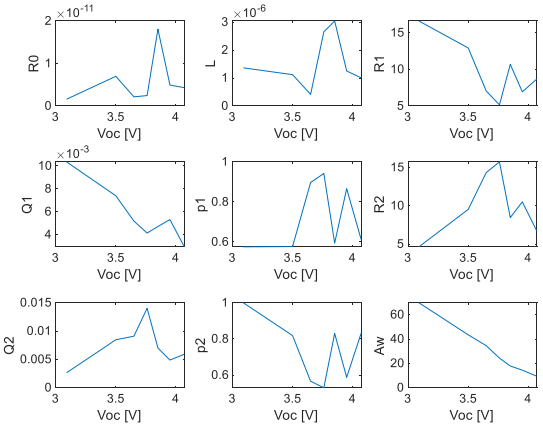

Fig. 22 – Behavior of the estimated parameters of Model 2 for the online monitoring data in the charging phase.

C. *Fitting online monitoring data*

The proposed fitting strategy is also applied to online monitoring data. Both the Model1 and Model2 are applied to the data obtained by the VIA in the online monitoring of a battery charging at constant current (see Sec. II-D). Fig. 19 and Fig. 20 show the fitting results for the two models while Fig. 21 and Fig. 22 show the related behavior of the estimated model parameters. A clear monotonic behavior of the p_1 and Q_1 parameters for Model1, and A_w parameter for Model2, may be observed, while the other parameters exhibit larger fluctuations. This suggests that *p1*, Q_1 and A_w parameters are suitable candidates for online monitoring of the state of charge of the battery cell.

IV. Conclusion

This paper proposes a compact system able to gather EIS data of lithium-ion batteries and estimate the target parameters of interest by using suitable electrical models. The proposed system could potentially operate "*online*", that is while the battery is under operation, and could be integrated into the battery cell thanks to its compactness, low power consumption, and isolation from the battery under test. Compactness and *online* operation of the proposed system could enable the development of built-in battery management systems, fault warning solutions, and real-time diagnostics.

The system is composed of a low-power vector impedance analyzer gathering raw impedance estimates, and a parameter estimator based on equivalent circuit models. Specifications

Tab. II Summary of prototype performance and specifications

Size	Frequency range	Max I_{peak}	Total Power	ASIC Power	Worst RMSE in cross-validation	RMSE of fitting to model 1	RMSE of fitting to model 2
3-cm x 6-cm	12 Hz – 45 kHz	1 mA	100 mW	1.45 mW	0.15 %RDG	0.22 Ω	0.17 Ω

This item was downloaded from IRIS Università di Bologna (https://cris.unibo.it/)

When citing, please refer to the published version.

and performances of the realized prototype are summarized in Table II. The realized VIA prototype was shown to provide experimental EIS results that are consistent with those of a reference laboratory instrument. The VIA prototype was validated in the online monitoring of a LIR2032 LIB cell during both charge and discharge cycle to prove the online capabilities of the measurement system. It was also compared to a reference instrument in the monitoring of aging effects, reporting consistent results. A modeling approach was applied to the measured data, showing that the parameters of the equivalent circuit model can be estimated based on measurements obtained by the realized VIA, and that the model provides a good fit to experimental data. Further measurement campaigns showed that the VIA correctly identifies trends in the model parameters, which are related to SoC levels.

Therefore, the proposed compact system is suitable for battery management applications and could further be integrated into a single chip. Potentially, the measurement system can be embedded within the battery cell to realize an efficient and low-power measurement system able to online estimate state parameters of the target battery.

REFERENCES

[1] H. M. Barkholtz, A. Fresquez, B. R. Chalamala, and S. R. Ferreira, "A Database for Comparative Electrochemical Performance of Commercial 18650-Format Lithium-Ion Cells," *J. Electrochem. Soc.*, vol. 164, no. 12, pp. A2697–A2706, 2017.

[2] A. Guha and A. Patra, "Online Estimation of the Electrochemical Impedance Spectrum and Remaining Useful Life of Lithium-Ion Batteries," *IEEE Trans. Instrum. Meas.*, vol. 67, no. 8, pp. 1836–1849, 2018.

[3] B. O. Agudelo, W. Zamboni, E. Monmasson, and G. Spagnuolo, "Identification of battery circuit model from EIS data," in *Conférence nationale des Jeunes Chercheurs en Génie Electrique & Rencontre annuelle du GDR SEEDS Énergie électrique pour le transport aérien*, 2019, pp. 11–14.

[4] H. Dai, B. Jiang, and X. Wei, "Impedance Characterization and Modeling of Lithium-Ion Batteries Considering the Internal Temperature Gradient," *Energies*, vol. 11, no. 1, p. 220, Jan. 2018.

[5] R. Al Nazer, V. Cattin, P. Granjon, M. Montaru, and M. Ranieri, "Broadband identification of battery electrical impedance for HEVs," *IEEE Trans. Veh. Technol.*, vol. 62, no. 7, pp. 2896–2905, 2013.

[6] A. De Angelis, J. Schoukens, K. R. Godfrey, and P. Carbone, "Practical Issues in the Synthesis of Ternary Sequences," *IEEE Trans. Instrum. Meas.*, vol. 66, no. 2, pp. 212–222, Feb. 2017.

[7] A. De Angelis, J. Schoukens, K. Godfrey, and P. Carbone, "Best Linear Approximation of Wiener Systems Using Multilevel Signals: Theory and Experiments," *IEEE Trans. Instrum. Meas.*, vol. 67, no. 5, pp. 1246–1253, May 2018.

[8] M. Crescentini, M. Bennati, and M. Tartagni, "A high resolution interface for Kelvin impedance sensing," *IEEE J. Solid-State Circuits*, vol. 49, no. 10, pp. 2199–2212, Oct. 2014.

[9] G. Luciani, R. Ramilli, A. Romani, M. Tartagni, P. A. Traverso, and M. Crescentini, "A miniaturized low-power vector impedance analyser for accurate multi-parameter measurement," *Meas. J. Int. Meas. Confed.*, vol. 144, pp. 388–401, Oct. 2019.

[10] E. Ravagli, M. Crescentini, P. Rovatti, and S. Severi, "Noninvasive Estimation of Plasma Sodium Concentration during Hemodialysis via Capacitively Coupled Electrical Impedance Spectroscopy," *IEEE Trans. Instrum. Meas.*, vol. 69, no. 4, pp. 1673–1681, Apr. 2020.

[11] C. P. Grey and J. M. Tarascon, "Sustainability and in situ monitoring in battery development," *Nature Materials*, vol. 16, no. 1. Nature Publishing Group, pp. 45–56, 20-Dec-2016.

[12] H. Yamauchi *et al.*, "Enhanced rate capabilities in a glass-ceramic-derived sodium all-solid-state battery," *Sci. Rep.*, vol. 10, no. 1, pp. 1–12, Dec. 2020.

[13] Q. K. Wang, Y. J. He, J. N. Shen, X. S. Hu, and Z. F. Ma, "State of Charge-Dependent Polynomial Equivalent Circuit Modeling for Electrochemical Impedance Spectroscopy of Lithium-Ion Batteries," *IEEE Trans. Power Electron.*, vol. 33, no. 10, pp. 8449–8460, 2018.

[14] M. Itagaki, K. Honda, Y. Hoshi, and I. Shitanda, "In-situ EIS to determine impedance spectra of lithium-ion rechargeable batteries during charge and discharge cycle," *J. Electroanal. Chem.*, vol. 737, pp. 78–84, Jan. 2015.

[15] U. R. Koleti, T. Q. Dinh, and J. Marco, "A new on-line method for lithium plating detection in lithium-ion batteries," *J. Power Sources*, vol. 451, p. 227798, Mar. 2020.

[16] E. Din, C. Schaef, K. Moffat, and J. T. Stauth, "A scalable active battery management system with embedded real-time electrochemical impedance spectroscopy," *IEEE Trans. Power Electron.*, vol. 32, no. 7, pp. 5688–5698, 2017.

[17] M. A. Varnosfaderani and D. Strickland, "Online impedance spectroscopy estimation of a dc–dc converter connected battery using a switched capacitor-based balancing circuit," *J. Eng.*, vol. 2019, no. 7, pp. 4681–4685, Jul. 2019.

[18] R. Ferrero *et al.*, "Low-Cost Battery Monitoring by Converter-Based Electrochemical Impedance Spectroscopy," in *AMPS 2017 - IEEE International Workshop on Applied Measurements for Power Systems, Proceedings*, 2017.

[19] J. A. A. Qahouq, "Online battery impedance spectrum measurement method," in *Conference Proceedings - IEEE Applied Power Electronics Conference and Exposition - APEC*, 2016, vol. 2016-May, pp. 3611–3615.

[20] W. Huang and J. A. Qahouq, "An online battery impedance measurement method using DC-DC power converter control," *IEEE Trans. Ind. Electron.*, vol. 61, no. 11, pp. 5987–5995, 2014.

[21] U. Troltzsch and O. Kanoun, "Miniaturized Impedance Measurement System for Battery Diagnosis | Semantic Scholar," in *Proc. SENSOR 20092*, 2009, pp. 251–256.

[22] D. A. Howey, P. D. Mitcheson, V. Yufit, G. J. Offer, and N. P. Brandon, "Online measurement of battery impedance using motor controller excitation," *IEEE Trans. Veh. Technol.*, vol. 63, no. 6, pp. 2557–2566, 2014.

This item was downloaded from IRIS Università di Bologna (https://cris.unibo.it/)

When citing, please refer to the published version.

[23] Z. Gong *et al*., "IC for online EIS in automotive batteries and hybrid architecture for high-current perturbation in low-impedance cells," in *Conference Proceedings - IEEE Applied Power Electronics Conference and Exposition - APEC*, 2018, vol. 2018-March, pp. 1922–1929.

[24] A. De Angelis *et al.*, "A Compact System for On-line Electrochemical Impedance Spectroscopy on Lithium-Ion Batteries," in *2020 IEEE International Instrumentation and Measurement Technology Conference (I2MTC)*, 2020, pp. 1–6.

[25] I. Landa-Medrano, I. Ruiz De Larramendi, N. Ortiz-Vitoriano, R. Pinedo, J. Ignacio Ruiz De Larramendi, and T. Rojo, "In situ monitoring of discharge/charge processes in Li-O2 batteries by electrochemical impedance spectroscopy," *J. Power Sources*, vol. 249, pp. 110–117, Mar. 2014.

[26] S. M. M. Alavi, C. R. Birkl, and D. A. Howey, "Time-domain fitting of battery electrochemical impedance models," *J. Power Sources*, vol. 288, pp. 345–352, Aug. 2015.

[27] A. A. Moya, "Identification of characteristic time constants in the initial dynamic response of electric double layer capacitors from high-frequency electrochemical impedance," *J. Power Sources*, vol. 397, pp. 124–133, Sep. 2018.

[28] J. J. Moré and D. C. Sorensen, "Computing a Trust Region Step," *SIAM J. Sci. Stat. Comput.*, vol. 4, no. 3, pp. 553–572, Sep. 1983.

[29] C. S. Cheng, H. S. H. Chung, R. W. H. Lau, and K. Y. W. Hong, "Time-Domain Modeling of Constant Phase Elements for Simulation of Lithium Battery Behavior," *IEEE Trans. Power Electron.*, vol. 34, no. 8, pp. 7573–7587, Aug. 2019.

[30] M. Galeotti, L. Cinà, C. Giammanco, S. Cordiner, and A. Di Carlo, "Performance analysis and SOH (state of health) evaluation of lithium polymer batteries through electrochemical impedance spectroscopy," *Energy*, vol. 89, pp. 678–686, Sep. 2015.

This item was downloaded from IRIS Università di Bologna (https://cris.unibo.it/)

When citing, please refer to the published version.